Article

Cyclometalated Iridium Complex-Based Label-Free Photoelectrochemical Biosensor for DNA Detection by Hybridization Chain Reaction Amplification

Chunxiang Li, Hongyang Wang, Jing Shen, and Bo Tang

Anal. Chem., **Just Accepted Manuscript** • Publication Date (Web): 27 Mar 2015

Cyclometalated Iridium Complex-Based Label-Free Photoelectrochemical Biosensor for DNA Detection by Hybridization Chain Reaction Amplification

Chunxiang Li,[†, ‡] Hongyang Wang,[‡] Jing Shen,[‡] Bo Tang*[,†]

[†]College of Chemistry, Chemical Engineering and Materials Science, Collaborative Innovation Center of Functionalized Probes for Chemical Imaging in Universities of Shandong, Key Laboratory of Molecular and Nano Probes, Ministry of Education, Shandong Provincial Key Laboratory of Clean Production of Fine Chemicals, Shandong Normal University, Jinan 250014, P.R. China.

[‡]Key Laboratory of Sensor Analysis of Tumor Marker Ministry of Education, College of Chemistry and Molecular Engineering, Qingdao University of Science and Technology, Qingdao 266042, P.R. China

ABSTRACT: Photoactive material is the most crucial factor which intimately determines analytical performances of the photoelectrochemical sensor. Based on high affinity of dipyrido [3,2-a:2',3'-c] phenazine (dppz) with DNA helix, a novel photoactive intercalators, $[(ppy)_2Ir(dppz)]^+PF_6^-$(ppy = 2-phenylpyridine and dppz = dipyrido [3,2-a:2',3'-c] phenazine) was prepared and characterized by UV−vis absorption spectroscopy, fluorescence spectrum and cyclic voltammetry. The photoelectrochemical properties of the as-prepared iridium(III) complex immobilized on the ITO electrode was investigated. Either cathodic or anodic photocurrent generation can be observed when triethanolamine (TEOA) or dissolved O_2 is used as a sacrificial electron donor/acceptor, respectively. The probable photocurrent-generation mechanisms are speculated. A highly sensitive iridium(III) complex-based photoelectrochemical sensor was proposed for DNA detection via hybridization chain reaction (HCR) signal amplification. Under optimal conditions, the biosensor was found to be linearly proportional to the logarithm of target DNA concentration in the range from 0.025 to 100 pmol L^{-1} with a detection limit of 9.0 fmol L^{-1} (3σ). Moreover, the proposed sensor displayed high selectivity and good reproducibility, demonstrating efficient and stable photoelectric conversion ability of the Ir(III) complex.

Photoelectrochemical sensing as a newly emerged yet promising technique has received substantial interest in biological analysis.[1] Due to the reduced background signals resulted from the complete separation of excitation source (light) and detection signal (current), it possesses potentially higher sensitivity than conventional optical and electrochemical methods. Moreover, benefiting from the utilization of electronic readout, this technique also shows some obvious advantages, including simple instrument, low cost, and easy miniaturization. As a result, a variety of photoelectrochemical sensing systems have been developed to detect biologically important species in the past decade.[2] Since the performance of the photoelectrochemical sensors depends intimately on the properties of the photoactive materials utilized, much effort has been devoted to design and synthesize novel materials, and the various active species, such as semiconducting nanoparticles, organic small molecules, and metal complexes, have been investigated for photoelectrochemical study to meet particular demand. Among them, metal complex is an important branch due to their thermal and photochemical stability, highly applicable photophysical and redox properties. So far, most of photoelectrochemical platforms about metal complexes have only focused on ruthenium complexes. Since Takagi et al. reported ruthenium complex as intercalator for the photoelectrochemical detection of double-strand DNA,[3] Guo et al. designed a series of ruthenium complexes-based photoelectrochemical detection system for various targets, including biotin/avidin recognition, the nucleotide, and DNA-damage.[4] Gao et al. synthesized a photoactive threading bis-intercalator consisting of two N,N'-bis(3-propyl-imidazole)-1,4,5,8-naphthalene diimides (PIND) linked by a $Ru(bpy)_2^{2+}$ (bpy = 2,2'-bipyridine) complex (PIND–Ru–PIND) for photoelectrochemical detection of the target nucleic acids.[2(a)] Haddour et al. synthesized ruthenium complex appended with electropolymerizable pyrrole groups and biotin as affinity binding groups for detection of anti-cholera toxin antibody.[2(b)] Liu et al. developed a photoelectrochemical method for double-stranded DNA detection using a high-affinity DNA intercalator, $Ru(bpy)_2dppz$ (dppz = dipyrido[3,2-a:2',3'-c]phenazine) as the signal indicator.[5] Compared with the extensive research on ruthenium complexes, less attention has been paid on the photoelectrochemical properties of iridium complexes despite their outstanding properties very similar to ruthenium complexes.

In the past decades, iridium complexes have extensively been utilized to organic light-emiting diodes,[6] electrogenerated chemiluminescence,[7] and light-emitting electrochemical cells,[8] thanks to their many merits, such as high luminescence efficiency, stability, tunable photophysical properties and diverse excited-state characteristics. Especially, compared to Ru complexes, Ir(III) complexes possess greater flexibility on structural design of coordinated ligands, which render them more flexible photoelectrochemical performances and could be used to detection of more diverse species. Recently, Cosnier's group demonstrated a novel cyclometallated Ir(III) complex

[bis(2-phenylpyridyl)(pyrrole-etherbipyridyl)Ir(III)]PF_6 exhibits similar photoelectrochemical properties and comparable photocurrent efficiency to [bis(bipyridyl)(pyrroleether bipyridyl) Ru(II)]$(PF_6)_2$ complex.[9] It generates anodic photocurrents in the presence of sodium ascorbate as a redox sacrificial donor, and cathodic photocurrents with methylviologen and oxygen as acceptors. Inspired by this report, we envision that novel iridium complexes-based photoelectrochemical active species with improved and stable photocurrents probably can be achieved by proper choice of the coordinated ligands.

Herein, we prepared a cationic Ir(III) complex, $[(ppy)_2Ir(dppz)]^+PF_6^-$ (ppy = 2-phenylpyridine), where ppy is the most traditional cyclometallated ligand, and the selection of dppz is based on its planar structure, which could render the complex to intercalate between the base pairs of a DNA helix with high affinity.[10] The UV-vis absorption, fluorescence, and photoelectrochemical properties of the as-prepared complex were investigated. Using the Ir(III) complex as intercalated reporter, a facile and effective photoelectrochemical sensing platform was established for sensitive determination of target DNA via the amplification of the hybridization chain reaction (HCR). To our knowledge, it is the first example that iridium complex-based photoelectrochemical sensor was established. We anticipate that this precursor study will be useful for exploiting excellent iridium complexes-based photoactive materials to achieve ultrasensitive detection platform.

EXPERIMENTAL SECTION

Materials and Reagents. Indium tin oxide (ITO) slices (ITO coating 180 ± 25 nm, sheet resistance ⩽10 Ω/square) were purchased from Weiguang Corp. (China). $IrCl_3 \cdot 3H_2O$, 2-phenylpyridine (ppy), 1,10-phenanthroline, o-phenylenediamine were purchased from Aladdin. Triethanolamine (TEOA), 6-Mercapto-1-hexanol (MCH), 3-mercaptopropyltrimethoxysilane (MPTMS) and tris(2-carboxyethyl) phosphine hydrochloride (TCEP) were obtained from Fluka. Tetrabutyl ammonium hexafluorophosphate (Bu_4NPF_6) was obtained from JK (China). Other reagents were all of analytical grade and used without further purification. Phosphate buffered solutions (PBS, 0.1 mol L^{-1} and 0.01 mol L^{-1}) were prepared by mixing the stock solutions of NaH_2PO_4 and Na_2HPO_4. Doubly distilled water was used in all experiments. Manipulations relating to Ir(III) complexes were carried out under nitrogen atmosphere, although they are air stable, due to the possible oxidation and thermal decomposition during the reactions. All of synthetic oligonucleotides were prepared from SBS Genetech Co. Ltd with the following sequences: Capture DNA (thiolated capture DNA immobilized on the electrode through Au-S bond, Cp-DNA): 5'-SH TAT TAA CTT TAC TCC-3'; C-DNA (complementary to Cp-DNA): 5'-GGA GTA AAG TTA ATA-3'; Target DNA: 5'-TCA GCG GGG AGG AAG GGA GTA AAG TTA ATA-3'; hairpin DNA H1: 5'-CTT CCT CCC CGC TGA CAA AGT TCA GCG GGG-3'; hairpin DNA H2: 3'-GTT TCA AGT CGC CCC GAA GGA GGG GCG ACT-5'; single-base mismatch DNA: 5'-TCA GCG GGG AGG AAG GGA GTA AAT TTA ATA-3'; noncomplementary DNA: 3'-GCG GCC TGG GCT GAA ACC AAC TTT ATT CAG-5'.

Apparatus. ^1H NMR spectra were recorded on a Bruker Avance 500 spectrometer using tetramethylsilane (TMS) as an internal standard. The UV/Vis absorption spectra were recorded on a Shimadzu UV-2600 spectrometer. The PL spectra were recorded on a Hitachi FL-4500 fluorescence spectrometer, and were carried out in thoroughly degassed CH_3CN. Cyclic voltammetry was carried out using an electrochemical workstation (CHI 660C). A three-electrode assembly was used with glassy carbon disk (diameter 2 mm) as the working electrode, a platinum wire as the counter electrode, and $Ag/AgNO_3$ (Ag/Ag^+) as the reference electrode in anhydrous CH_3CN containing 0.1 mol L^{-1} Bu_4NPF_6 as the supporting electrolyte. The potential was calibrated against an aqueous SCE using ferrocene (Fc) as an external standard, where $E_{1/2}$ (Fc^+/Fc) = 0.40 V vs. SCE.[11] Electrochemical impedance spectroscopy (EIS) was performed on an electrochemical workstation (CHI 660C) with a three-electrode system in 0.1 mol L^{-1} pH 7.4 PBS containing 10 mmol L^{-1} $Fe(CN_6)^{3-/4-}$ (1:1) as the redox probe, and recorded in the frequency range of 0.01 Hz to 100 kHz under an oscillation potential of 5 mV. Photoelectrochemical measurements were performed with MPI-EO photoelectrochemical analysis system (Xi'an Remex Analysis Instrument Co. Ltd. Xi'an, China). A 150-W Xe lamp equipped with omni-λ 150 monochromator (Zolix) was used as the irradiation source. A conventional three-electrode system were equipped with a modified ITO (0.25 cm^2) as the working electrode, a platinum wire as the auxiliary electrode, and a saturated Ag/AgCl electrode as the reference electrode.

Synthesis of the Ligand dppz and the Complex $[(ppy)_2Ir(dppz)]^+PF_6^-$. The ligand dppz and the complex $[(ppy)_2Ir(dppz)]^+PF_6^-$ were synthesized according to the literature methods with appropriate modifications (see the Supporting Information).[10(b),12,13]

Preparation of $[(ppy)_2Ir(dppz)]^+PF_6^-$ Modified ITO Electrode. ITO electrode was cleaned with NaOH (1 mol L^{-1}) and H_2O_2 (30%), then washed successively with acetone, ethanol, and twice-distilled water under ultrasonication, and dried at room temperature. 10 μL of the $[(ppy)_2Ir(dppz)]^+PF_6^-$ solution in CH_3CN (1×10^{-4} mol L^{-1}) was spread dropwised on the ITO electrode with a syringe and dried at room temperature. The photoelectrochemical properties of the thus-obtained electrodes were measured in PBS solution (pH = 7.4).

Preparation of AuNPs. AuNPs were prepared according to the method reported previously with a slight modification.[14] 10 mL of 38.8 mmol L^{-1} trisodium citrate solution was added to 100 mL of boiling 1.0 mM $HAuCl_4$ solution quickly and stirred for 10 min under refluxing. The color of the solution changed from pale yellow to wine red in the end, which was an indication for the formulation of the AuNPs. After refluxed for an additional 15 min, the nanoparticle solution was allowed to cool down to room temperature with continuously stirring. The particles were examined by UV-vis absorption spectra and characterized by absorption maximum at 510 nm, which corresponds to the size of ca. 20 nm. The as-prepared AuNPs was kept away from light in freezer (4 °C) for the next use.

Preparation of Intercalated $[(ppy)_2Ir(dppz)]^+PF_6^-$ Modified ITO Electrode. After cleaning according to the method above, the ITO electrode was immersed in 5% MPTMS ethanol solution overnight. Thus, the ITO surface was functionalized with an SH-rich self-assembled layer. After careful rinsing with ethanol, the ITO electrode was heated to 80 °C to remove loosely bound MPTMS molecules in order to prevent gold nanoparticle aggregates in the next step. Then, the SH-modified electrode was immersed in above-prepared AuNPs (10-fold diluted) for 10 h at room temperature. After rinsing

with excess twice-distilled water, the AuNP-modified electrode was ready for further experiments. Cp-DNA (activation with TCEP, 10^{-6} mol L^{-1}, 20 μL) was dropped on the above AuNP-modified ITO electrode for 6 h at 37 °C. Then, it was rinsed thoroughly with PBS buffer (0.01 mol L^{-1}, pH = 7.4) to remove any weakly absorbed Cp-DNA. 50 μL of MCH (10^{-3} mol L^{-1}) was used to saturate the possible bare AuNPs for 1 h at 37 °C and flushed with 0.01 mol L^{-1} PBS buffer. C-DNA (10^{-8} mol L^{-1}, 20 μL) was dropped on the electrode modified with Cp-DNA, and incubated for 1 h at 37 °C, subsequently washed with copious amounts of PBS buffer. Finally, the as-modified electrode with ds-DNA was immersed in $[(ppy)_2Ir(dppz)]^+PF_6^-$ solution (5×10^{-5} mol L^{-1}, 200 μL, CH_3CN : PBS (0.1 mol L^{-1}) = 1 : 1 (V/V)) for 0.5 h. The resulting electrode was washed adequately with PBS buffer to clean off the unbinding $[(ppy)_2Ir(dppz)]^+PF_6^-$. The photoelectrochemical properties of the thus-obtained electrodes were measured with or without electron donor in 0.1 mol L^{-1} PBS solution (pH = 7.4) irradiated with 380 nm light.

Fabrication of the DNA Sensor. The cleaning of the ITO electrode and further modification with AuNPs and Cp-DNA were carried out according to the same way as above. Prior to use, the hairpin DNA H1 and H2 were heated to 95 °C for 2 min and then allowed to cool to room temperature for 1 h. The prepared Cp-DNA modified electrode was soaked in 20 μL target DNA solution at various concentrations for 2 h. After rinsing with PBS buffer and air drying, the prepared electrode was incubated with a mixture of 10 μL H1 (10^{-6} mol L^{-1}) and 10 μL H2 (10^{-6} mol L^{-1}) in the reaction buffer for 2 h, and then rinsed with PBS buffer and air dried. The as-prepared ds-DNA modified electrode was immersed in $[(ppy)_2Ir(dppz)]^+PF_6^-$ solution (5×10^{-5} mol L^{-1}, 200 μL) and incubated for 0.5 h and then washed with PBS buffer to remove the nonspecifically adsorbed complexes.

Photoelectrochemical Measurement. The photocurrent intensity of the resulting functionalized electrode was recorded in 0.1 mol L^{-1} PBS solution (pH = 7.4) containing 0.1 mol L^{-1} TEOA as sacrificial electron donor during the photocurrent measurement irradiated with 380 nm light. The light was switched on and off every 20 s and the applied potential was 0.1 V.

RESULTS AND DISCUSSION

Electronic Absorption, Fluorescence and Electrochemical Properties. The absorption and emission spectra at ambient temperature in CH_3CN are shown in Figure 1. The complex showed intense intraligand (^{1}IL ($\pi\rightarrow\pi^*$ (dppz and ppy)) absorption bands ($\varepsilon > 10^4$ dm^3 mol^{-1} cm^{-1}) at approximately 270, 342, 365 and 384 nm. The complex also displayed weak absorption at around 468 nm attributed to metal-to-ligand charge transfer (MLCT) ($d\pi$ (Ir)$\rightarrow\pi^*$ (dppz and ppy)) transitions with reference to previous photophysical studies on related iridium(III) systems,[15] which is similar to that of Ru(II) complex (Figure S1, see the Supporting Information). The absorption onset at 520 nm corresponds to a HOMO–LUMO energy difference of 2.38 eV according to $E_{0\text{-}0} = 1240/\lambda_{onset}$.[16]

Upon photoexcitation, the complex displayed phosphorescent emission with a maximum wavelength at 610 nm in CH_3CN. According to previous reports about this complex,[10(b)] the emission is assigned to ^{3}MLCT ($d\pi$ (Ir)$\rightarrow\pi^*$ (dppz) excited state. Quantum efficiency (Φ_m) of the complex was estimated to be 0.0065 with $Ru(bpy)_3^{2+}$ (Φ_m = 0.015) in CH_3CN as a reference (see the Supporting Information).[15(e)] The lower quantum yield is probably due to the hydrogen-bonding interactions between the diimine ligands and solvent molecules. The electrochemical properties of $[(ppy)_2Ir(dppz)]^+$ has been studied by cyclic voltammetry. The complex showed a couple of anodic couple at $E_{1/2}$ = +1.26 V with an onset oxidation potential of +1.18 V vs. SCE (Figure 1(B)), which was assigned to metal-centered Ir^{IV}/Ir^{III} oxidation. Also the complex exhibited reduction couples at −1.38 and −1.76 V vs. SCE (Figure S2, the Supporting Information), which were assigned to the reduction of the diimine ligands according to previous studies.[10(c), 17]

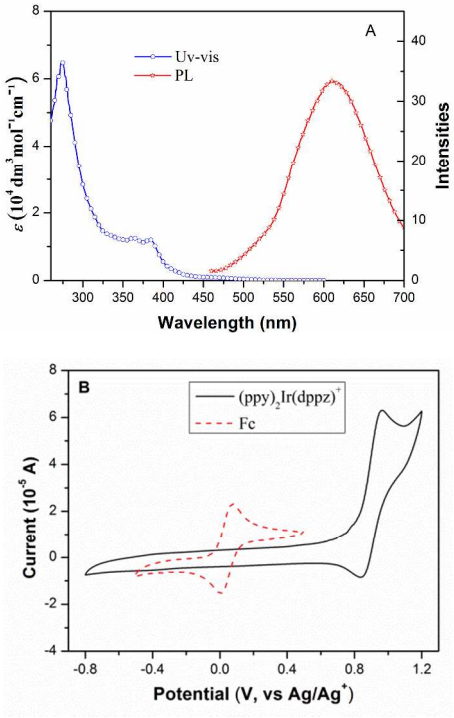

Figure 1 (A) Electronic absorption and emission spectra of $[(ppy)_2Ir(dppz)]^+PF_6^-$ (2×10^{-5} mol L^{-1}) in CH_3CN, the excited wavelength for the emission spectra is 375 nm. (B) Cyclic voltammograms of $[(ppy)_2Ir(dppz)]^+$ (10^{-3} mol L^{-1}) and Fc (10^{-5} mol L^{-1}, external standand) in anhydrous CH_3CN containing 0.1 mol L^{-1} Bu_4NPF_6 as the supporting electrolyte at 25 °C, glassy carbon electrode, scan rate, 100 mV s^{-1}.

Photoelectrochemical Property. The photoelectrochemical property for $[(ppy)_2Ir(dppz)]^+$ was investigated through coating it on the ITO electrode. Upon changing the excitation wavelength between 200−600 nm, a preliminary photocurrent action spectrum is obtained with a peak at around 380 nm, as shown in Figure S3 (see the Supporting Information) , which is coincident with the absorption spectrum of $[(ppy)_2Ir(dppz)]^+$, indicating that the complex coated on the ITO electrode is responsible for the photocurrent generation.

As shown in Figure 2(A), steady cathodic photocurrents were obtained from $[(ppy)_2Ir(dppz)]^+$ modified electrode when it was illuminated by a 380 nm light in 0.1 mol L^{-1} PBS solution (pH = 7.4). The photocurrent response was very stable under several on-off cycles of light irradiation without any bias voltage. The photocurrent dependence on an bias voltage potential of −0.3 ~ 0.3 V was investigated to understand the behavior of electron injection of $[(ppy)_2Ir(dppz)]^+$ (depicted in

Figure 2, curve a-g). From Figure 2(B), it is clearly found that the negative bias voltages applied have a great impact on the photocurrents, and the more negative the bias voltage, the greater the photocurrent. It probably could be attributed to an enhancement of the rate constant for charge transfer. When positive bias voltage was applied to the ITO electrode, cathodic photocurrent slowly decreases with the increase of bias voltage, which is maybe due to easier recombination of electron-hole pairs.[18] The dark current reveals a similar change tendency to the photocurrent. When positive or without bias voltage was applied, the dark current from $[(ppy)_2Ir(dppz)]^+$ modified ITO electrode is low or almost negligible, while a significant dark current was generated when applied bias voltage is negative, especially at −0.3 V. To reveal the reason of high dark current at high bias voltage, a control experiment was performed by measuring the photocurrent in the absence of $[(ppy)_2Ir(dppz)]^+$ in PBS at various bias voltages, the results was depicted in Figure S4 (see the Supporting Information). It indicated that high dark current does not arise from the direct electrochemical reduction of oxygen. It probably arises from electrochemical redox of Ir(III) complex according to similar behavior of $Ru(bpy)_3^{2+}$ and Re(I) complex reported previously.[19]

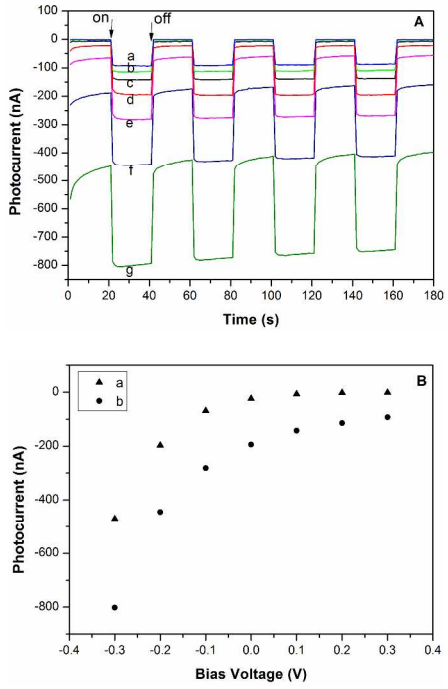

Figure 2 (A) Photocurrent responses induced by switching on and off the light (380 nm) irradiation from $[(ppy)_2Ir(dppz)]^+$ modified ITO electrode in 0.1 mol L^{-1} PBS solution (pH = 7.4) at applied bias voltage of (a) 0.3 V, (b) 0.2 V, (c) 0.1 V, (d) 0 V, (e) −0.1 V, (f) −0.2 V and (g) −0.3 V. (B) Plotting of photocurrent vs. bias voltage based on (A), (a) dark current (switch off) (b) photocurrent (switch on).

To further exploit the application of $[(ppy)_2Ir(dppz)]^+$ as a photoelectrochemical probe, photoelectrochemical behavior of the Ir(III) complex intercalated to double-stranded DNA was investigated. The assembly process of the modified electrode was illustrated in Scheme 1. After the ITO electrode was functionalized with MPTMS, AuNPs was immobilized through Au–S bond. Thiol-functionalized capture DNA (Cp-DNA) self-assembled on AuNPs modified ITO electrode through Au–S bond and hybridized with its complementary DNA (C-DNA) by the double-stranded. $[(ppy)_2Ir(dppz)]^+$, as photoelectrochemical signal reporter, was intercalated into the resulting ds-DNA structure attached to the electrode. The photoelectrochemical signal from the intercalated $[(ppy)_2Ir(dppz)]^+$ was investigated. As shown in Figure 3, steady cathodic photocurrents were generated in PBS solution under light irradiation at 380 nm without any bias voltage (curve a). Obviously, under several on-off cycles of light irradiation, the photocurrent responses were prompt and reproducible. To acquire optimal operating conditions, the photocurrent dependence on the bias voltage was investigated. From Figure 3(B), it was found that cathodic photocurrent increased with the increasing of negative bias voltage applied to the electrode. However, when applied bias voltage is at −0.2 V, a very obvious dark current appeared (curve b and c). To further understand the flow direction of electron through ds-DNA, the effect of the electron donor and bias voltage on $[(ppy)_2Ir(dppz)]^+$ modified ITO electrode were also investigated. Employing TEOA as sacrificial electron donor, very stable and reproducible anodic photocurrent was produced (curve d). When positive bias voltage was applied, a great increment of anodic photocurrent can be seen with the increase of bias voltage (curve e and f). In view of greater dark current at 0.2 V, 0.1 V of applied bias voltage is the optimum condition since generated photocurrents possess high efficiency, good stability and good reproducibility. The maximum incident photon to current conversion efficiency (IPCE) with TEOA as electron donor at 0.1 V bias voltage was derived to be to be 0.38% (see the Supporting Information), which is far more than the 0.065% of $[Ru(bpy)_2L](ClO_4)_2$ based multilayer film.[20]

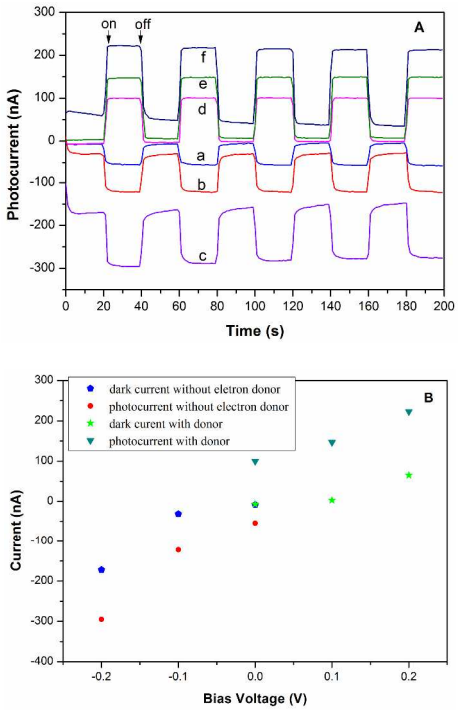

Figure 3 (A) Anodic (curve a–c) and cathodic (curve d–f) photocurrents from $[(ppy)_2Ir(dppz)]$+ intercalated into ds-DNA induced by switching on and off the light (380 nm) irradiation in 0.1 mol L^{-1} PBS solution (pH = 7.4) at applied bias voltage of (a) 0, (b) −0.1 V and (c) −0.2 V; and containing 0.1 mol L^{-1} TEOA as sacrificial electron donor at applied bias voltage of d) 0, (e) 0.1 V and (f) 0.2 V. (B) Plotting of current vs. bias voltage based on (A).

Scheme 1 Diagram for Assembling of Intercalated $[(ppy)_2Ir(dppz)]^+PF_6^-$ Modified ITO Electrode.

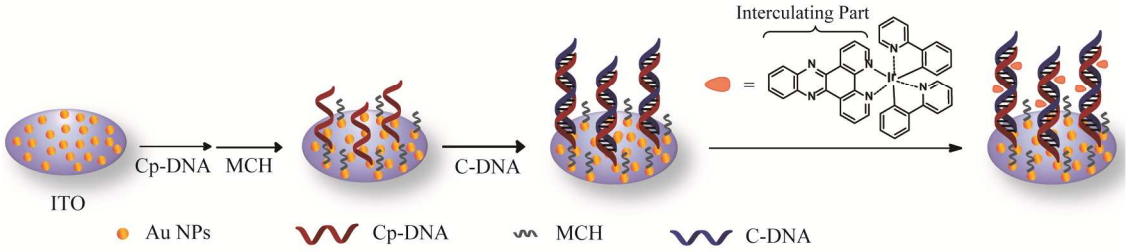

In order to have an insight into the mechanisms of cathodic and anodic photocurrent generation, the control experiments were carried out in both deoxygenated and air-equilibrated electrolyte solutions. As shown in Figure S5 (see the Supporting Information), when the electrolyte solution was deoxygenated through bubbling N_2 for 30 min, the photocurrent decreased sharply about 80%, suggesting dissolved O_2 played an important role in the process of anodic photocurrent generation. The small residual photocurrent was attributed to trace amount of residual O_2 in the electrolyte solution, which is hard to remove completely under our experimental conditions. In addition, excited-state redox potentials were estimated through cyclic voltammetry data and UV-vis absorption spectral to demonstrate the photocurrent generation. From an onset oxidation potential $E_{onset}(ox)$ at +1.18 V and the first onset reduction potential $E_{onset}(red)$ at −1.38 V, the excited state redox potentials of $Ir^{III}*/Ir^{IV}$ and $Ir^{III}*/Ir^{III,L^-}$ was determined to be −1.20 V and 1.0 V, respectively, according to the equations:[21]

$$E\,(Ir^{III}*/Ir^{IV}) = E_{onset}(Ir^{III}/Ir^{IV}) - E_{0\text{-}0} \quad (1)$$

$$E\,(Ir^{III,L}*/Ir^{III,L^-}) = E_{onset}\,(Ir^{III,L}/Ir^{III,L^-}) + E_{0\text{-}0} \quad (2)$$

Scheme 2 Proposed Mechanism of Photocurrent Generation. Solid lines and dotted lines represent cathodic and anodic photocurrent generation, respectively.

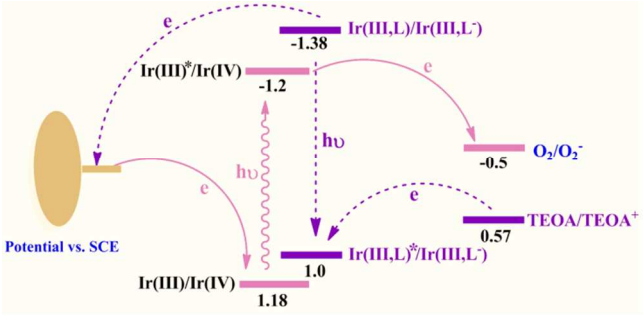

Using above-mentioned energy level values, the energy level diagram was thus constructed, and the proposed cathodic and anodic photocurrent generation mechanism is depicted in Scheme 2. The cathodic photocurrent probably involves the formation of the excited state $[(ppy)_2Ir(dppz)]^+*$ excited by the light irradiation and a subsequent electron transfer from the excited state $[(ppy)_2Ir(dppz)]^+*$ to the electron acceptor O_2 in the electrolyte solution. The electrode further donated an electron to regenerate the $[(ppy)_2Ir(dppz)]^+$ ground state, triggering the photocurrent generation. However, in presence of TEOA as electron donor, the excited state $[(ppy)_2Ir(dppz)]^+*$ was reduced by TEOA to $(ppy)_2Ir(dppz)$, which was demonstrated by emission quenching experiments (see the Supporting Information) and the quenching behavior is similar to that of the reported cationic iridium complexes.[22] Since Ir(II) is not electrochemically accessible, diimine ligands accept an electron to L^-.[23] The generated $(ppy)_2Ir(dppz)$ finally injects an electron into the electrode resulting in an anodic photocurrent.[9,24]

Fabrication of the DNA Sensor. HCR was first reported by Pierce et al. and has been extensively used for enzyme-free amplified detection of DNA with PCR-like sensitivity.[25] It is triggered by an initiator and form a long nicked ds-DNA polymer through a cascade of hybridization events between two helper DNA hairpins. Herein, we proposed a DNA detection system employing $[(ppy)_2Ir(dppz)]^+$ as intercalated indicator. As depicted in scheme 3, the protocol involves thiolfunctionalized Cp-DNA self-assembled on the AuNPs functioned ITO electrode. In the absence of target DNA, both hairpin H1 and H2 are in the closed form. The weak interaction between Ir(III) complex and the short ss-DNA causes a considerably low photoelectrochemical background signal. However, in the presence of target DNA, one end of it was captured with Cp-DNA self-assembled on the electrode, and the other end as the initiator to trigger the HCR. Therefore, a small amount of DNA, with the assistance of helper hairpins H1 and H2, can form long ds-DNAs, which permit the intercalation of numerous $[(ppy)_2Ir(dppz)]^+$ and achieve significantly amplified photoelectrochemical signals.

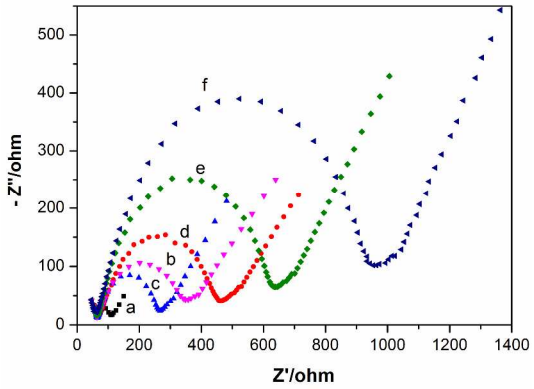

Figure 4 Electrochemical impedance spectroscopy of different electrodes (a) the bare ITO electrode; (b) ITO/MPTMS; (c) ITO/MPTMS/AuNPs; (d) ITO/MPTMS/AuNPs/Cp-DNA; (e) ITO/MPTMS/AuNPs/Cp-DNA/Target DNA; (f) ITO/MPTMS /AuNPs/Cp-DNA/Target DNA/H1 + H2. The spectra were recorded in 0.1 mol L^{-1} pH 7.4 PBS containing 10 mmol L^{-1} $Fe(CN_6)^{3-/4-}$as the redox probe, using a frequency of 100 KHz to 0.01 Hz under an oscillation potential of 5 mV.

EIS Monitoring of the Fabrication of the Sensor. Electrochemical impedance spectra (EIS) is an effective tool for probing the features of surface-modified electrodes. The EIS measurements of the modified ITO electrode at different modification steps were carried out and the results as Nyquist plot

Scheme 3 Illustration of the HCR-Based Strategy for Photoelectrochemical Detection of DNA.

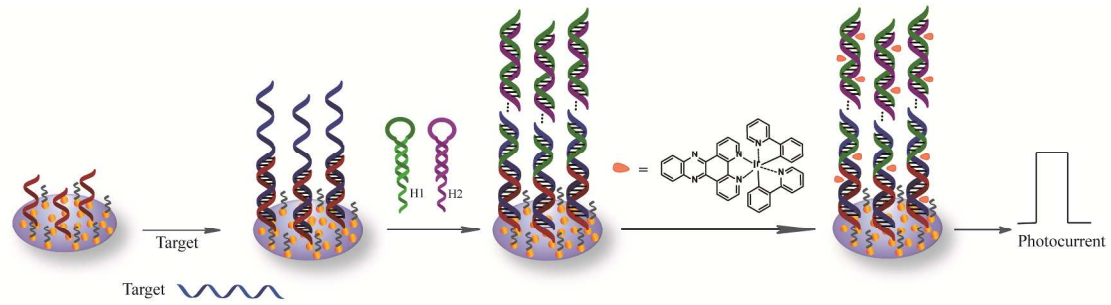

are illustrated in Figure 4, which showed a semicircle in the high-frequency region while showed a straight line in the low-frequency region, demonstrating that the electrode process was controlled by electron transfer at high frequency and by diffusion at low frequency. It could be seen that the bare ITO electrode exhibited the smallest Ret value (curve a). After functionalization with MPTMS, the ITO surface generated an insulating layer on the electrode surface, which resulted in obviously increased in Ret (curve b). The Ret value decreased when AuNPs were further assembling on the ITO/MPTMS electrode (curve c), which may be because the AuNPs could facilitate electron-transfer. Subsequently, when the modified electrode was assembled with the Cp-DNA (curve d) and further hybridized with target DNA (curve e), the diameter of semicircular part successively increased, suggesting the electron transfer of the redox probe was obstructed by the assembled DNA strands, which slowed down the redox reaction of$Fe(CN_6)^{3-/4-}$. Finally, when the assembled electrode was associated with H1 and H2, the polymerization of oligonucleotides leads to a remarkable increased electron transfer resistance (curve f). These results were consistent with the fact that the electrode was fabricated as expected.

Optimization of Assay Conditions. To achieve excellent performance in the photoelectrochemical assay for sensitive detection of DNA, the incubation time for the intercalation and the concentration of $[(ppy)_2Ir(dppz)]^+$ were optimized by monitoring the changes of the photocurrents. As shown in Figure 5(A), in the presence of target DNA, as intercalation proceeded, the anodic peak current increased due to increase of $[(ppy)_2Ir(dppz)]^+$ intercalated into ds-DNA immobilized on the electrode surface. After 30 min, the ds-DNAs tend to be saturated with $[(ppy)_2Ir(dppz)]^+$ molecules, and photocurrent reaches a plateau. At the same time, the influence of incubation time for intercalation on background current in the absence of the target DNA was also investigated, as seen in Figure 5(A), the background currents, resulting from nonspecific interaction with ss-DNA and electrode adsorption, increased slowly with the increment of incubation time. Since incubation time of 30 min renders the sensing system to reach the maximum signal-background ratio, it was selected for further investigation. Figure 5(B) shows the effect of $[(ppy)_2Ir(dppz)]^+$ concentration on the photocurrent in the presence and absence of target DNA. As can be seen, when the concentration is high enough, a maximum value of the peak current was obtained. While, incremental concentration also leads to increased background signal owing to stronger diffusion process. From the results, 6×10^{-5} mol L^{-1} concentration of $[(ppy)_2Ir(dppz)]^+$ complex was chosen as the optimum.

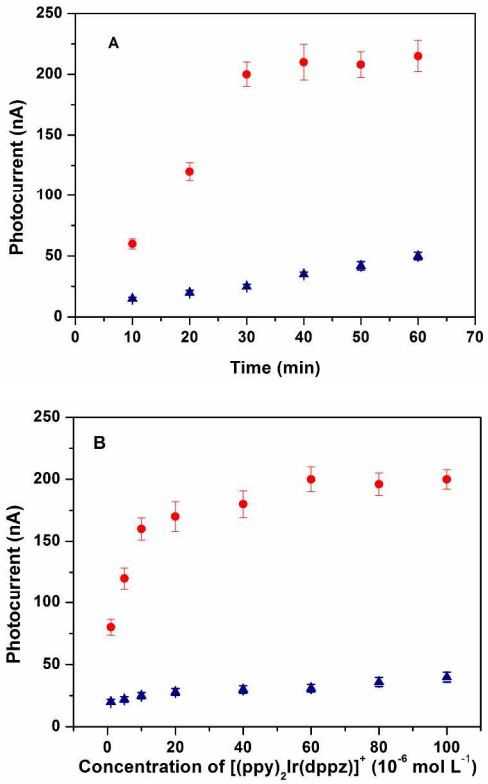

Figure 5 (A) Effect of incubation time for the intercalation of $[(ppy)_2Ir(dppz)]^+$ in the presence (●) and absence (▲) of target DNA; (B) Effect of concentration of $[(ppy)_2Ir(dppz)]^+$ in the presence (●) and absence (▲) of target DNA. The concentration of target DNA was 1.0×10^{-12} mol L^{-1}. Measurement was carried out in 0.1 mol L^{-1} PBS (pH = 7.4) containing 0.1 mol L^{-1} TEOA.

Analytical Performance of the Photoelectrochemical Sensor. On the basis of the strategy as stated above, this as-prepared photoelectrochemical sensor was applied to DNA detection. Under optimal conditions, photocurrent signals were measured at various concentrations of DNA with TEOA concentration of 0.1 mol L^{-1} and applied bias potential of 0.1 V. The photocurrent responses were measured by varying the target DNA concentrations, and the results were depicted in Figure 6(A). In the absence of target DNA, a relatively low photocurrent was obtained. As concentration of the target DNA increases, the photocurrents increased accordingly. The calibration plot was constructed by plotting photocurrent increment ($\Delta I = I - I_0$, where I and I0 represent the photocurrent intensity produced in the presence and absence of target DNA, respectively) against logarithm of DNA concentrations in a linear range from 0.025 to 100 pmol L^{-1} (Figure 6(B)) with a

correlation coefficient of 0.994. The detection limit was estimated to be 9.0 fmol L^{-1} at 3σ. For comparison, previously reported DNA detection protocols are presented in Table S1 (See the Supporting Information). This sensitivity of this work exceeds HCR amplification-based fluorescent and electrochemiluminescent method for DNA detection (250 and 15 fmol L^{-1}, respectively).[25(b,c)] Also, it increased nearly 2 order of magnitude compared to that of CdTe quantum dots-based photoelectrochemical sensor (0.8 pmol L^{-1}).[26] Obviously, the improved sensitivity of the proposed method can be attributed to both the excellent photoelectrochemical behavior of iridium complex and effective signal amplification strategy. The reproducibility of the proposed DNA sensor was evaluated by analyzing five independently fabricated electrodes. The photo current response offered a relative standard deviation (RSD) of 7.6% toward 5.0 × 10−14 mol L−1 target DNA, which indicated an acceptable accuracy and reproducibility of the assay.

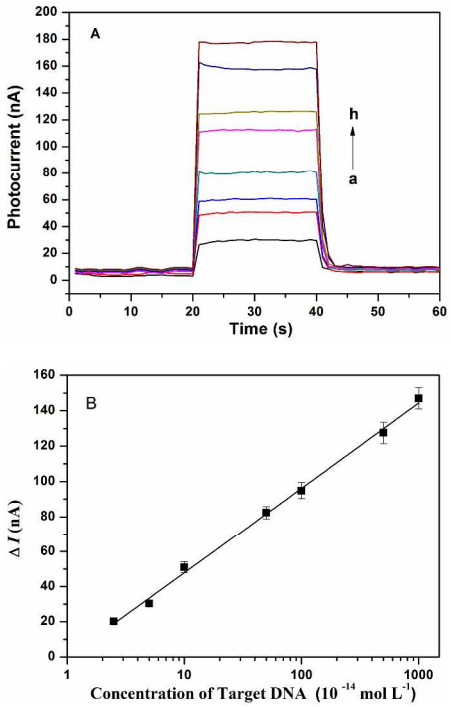

Figure 6 (A) Photocurrent responses of the sensor to different concentration of target DNA (a) 0, (b) 2.5 × 10^{-14} mol L^{-1}, (c) 5.0 × 10^{-14} mol L^{-1}, (d) 1.0 × 10^{-13} mol L^{-1}, (e) 5.0 × 10^{-13} mol L^{-1}, (f) 1.0 × 10^{-12} mol L^{-1}, (g) 5.0 × 10^{-12} mol L^{-1}, (h) 1.0 × 10^{-11} mol L^{-1}. Photocurrent measurement conditions, as in Figure 6; (B) The calibration curve of ΔI and logarithm of concentrations of target DNA using the present photoelectrochemical sensor. The error bars show the standard deviation of three replicate determinations. Measurement was the same as Figure 6.

The Selectivity of the Photoelectrochemical Sensor. The selectivity of the proposed sensor was evaluated by comparing the photocurrent response to different DNA sequences, including target DNA, single-base mismatched, and noncomplementary DNA at the concentrations of 5.0 × 10^{-14}, 5.0 × 10^{-13} and 5.0 × 10^{-12} mol L^{-1}, respectively. As shown in Figure 7, it can be seen that the photoelectrochemical responses of non-complementary DNA have no obvious difference compared to the control experiment in the absence of target DNA. Although the photocurrent increase in the presence of single-base mismatch DNA was observed owing to their hybridization with Cp-DNA, it was not comparable with that of the target DNA, suggesting that it couldn't open the hairpin to trigger the HCR process. These results demonstrated that the photocurrent response was specifically triggered by perfectly matched target DNA, suggesting that the proposed DNA assay could offer high specificity for nucleic acid detection.

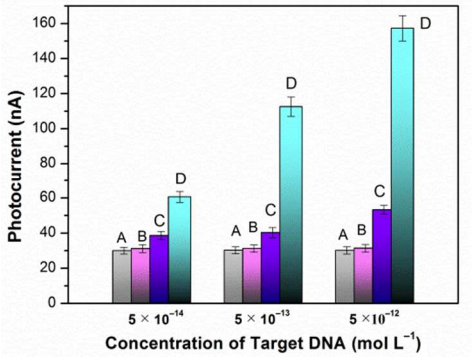

Figure 7 Selectivity investigation of the photoelectrochemical sensor for target DNA against different DNA sequences: (A) blank (in the absence of target DNA), (B) noncomplementary DNA, (C) single-base mismatch DNA and (D) target DNA. The error bars showed the standard deviation of three replicate determinations.

CONCLUSION

In summary, a novel photoelectrochemical active material, $[(ppy)_2Ir(dppz)]^+$ has been designed and synthesized. The photoelectrochemical property of the Ir(III) complex immobilized on ITO electrode through intercalating into double-stranded DNA has been investigated. As proven by our research, it exhibited stable cathodic photocurrent in the presence of O_2 as electron acceptor illuminated by 380 nm light, while in the presence of TEOA as redox sacrificial donor, it exhibited very stable and reproducible anodic photocurrent at +0.1 V bias potential. Probable mechanisms have been speculated through calculating the energy levels of the HOMO and LUMO. Moreover, employing $[(ppy)_2Ir(dppz)]^+$ as intercalated signal reporter, a photoelectrochemical sensor has been fabricated for DNA detection based on HCR signal amplification for the first time. Benefiting from excellent photoelectrochemical performance of the Ir(III) complex and the amplifying functionality of HCR, the proposed method exhibits high sensitivity at the femtomolar level. And, this label-free detection approach is also coupled with high selectivity and good reproducibility. Our study shows that this series of easily synthetic, air-stable and conveniently tunable Ir(III) complexes are the promising candidates for photoactive materials. It is expected that further improved iridium(III) complexes through the rational molecular design could be used in more fields for biological assays and clinical diagnoses.

ASSOCIATED CONTENT

Supporting Information

Additional information as noted in text. This material is available free of charge via the Internet at http://pubs.acs.org.

AUTHOR INFORMATION

Corresponding Author

*E-mail: tangb@sdnu.edu.cn. Fax: +86 531 86180017.

Notes

The authors declare no competing financial interest.

ACKNOWLEDGMENT

This work was financially supported by 973 Program (2013CB933800), the Natural Science Foundation of China (no. 21227005, 21390411, 91313302 and 21205065) and the Postdoctoral Science Foundation of China (no. 2012M521371).

REFERENCES

(1) (a) Willner, I.; Patolsky, F.; Wasserman, J. *Angew. Chem. Int. Ed.* **2001**, *40*, 1861−1864. (b) Zhang, X. R.; Guo, Y. S.; Liu, M. S.; Zhang, S. S. *RSC Adv.* 2013, *3*, 2846−2857. (c) Zhao ,W. W.; Xu, J. J.; Chen H. Y. *Chem. Rev.* **2014**, *114*, 7421−7441. (d) Long, Y. T.; Kong, C.; Li, D. W.; Li, Y.; Chowdhury, S.; Tian, H. *Small*, **2011**, *7*, 1624–1628.

(2) (a) Gao, Z. Q. ; Tansil, N. C. *Nucleic Acids Res.* **2005**, *33*, e123. (b) Tu, W. W.; Dong, Y. T.; Lei, J. P.; Ju, H. X. *Anal. Chem.* **2010**, *82*, 8711–8716. (c) Haddour, N.; Chauvin, J.; Gondran C.; Cosnier, S. *J. Am. Chem. Soc.* **2006**, *128*, 9693–9698. (d) Wu, S.; Song, H. L.; Song, J.; He, C.; Ni, J.; Zhao, Y. Q.; Wang, X. Y. *Anal. Chem.* **2014**, *86*, 5922−5928. (e) Hojeij, M.; Su, B.; Tan, S. X.; Me´riguet G.; Girault, H. H. *ACS Nano*. **2008**, *2*, 984–992. (f) Zhang, B.; Guo, L.-H.; Greenberg, M. M. *Anal. Chem.* **2012**, *84*, 6048−6053. (f) Zeng, X. X.; Tu, W. W.; Li, J.; Bao, J. C.; Dai, Z. H. *ACS Appl. Mater. Interfaces* **2014**, *6*, 16197–16203. (g) *Anal. Chem.* **2012**, *84*, 10518−1052. (h) Zhao, W.-W.; Ma, Z.-Y.; Xu, J.-J.; Chen H.-Y. *Anal. Chem.* **2013**, *85*, 8503−8506. (i) Fan, G.-C.; Han, L.; Zhu, H.; Zhang, J.-R.; Zhu, J.-J. *Anal. Chem.* **2014**, *86*, 12398–12405. (j) Zhao, W.-W.; Chen, R.; Dai, P.-P.; Li, X.-L.; Xu, J.-J.; Chen, H.-Y. *Anal. Chem.* **2014**, *86*, 11513–11516.

(3) Nakamura, S.; Shibata, A.; Takenaka, S.; Takagi, M. *Anal. Sci.* **2001**, *17*, i431.

(4) (a) Dong, D.; Zheng, D.; Wang, F.-Q.; Yang, X.-Q.; Wang, N.; Li, Y.-G.; Guo, L.-H.; Cheng, J. *Anal. Chem.* **2004**, *76*, 499−501. (b) Liang, M. M.; Liu, S. L.; Wei, M. Y.; Guo, L.-H. *Anal. Chem.* **2006**, *78*, 621−623. (c) Liang, M. M.; Jia, S. P.; Zhu, S. C.; Guo, L.-H. *Environ. Sci. Technol.* **2008**, *42*, 635–639. (d) Jia, S. P.; Liang, M. M.; Guo, L.-H. *J. Phys. Chem. B* **2008**, *112*, 4461−4464. (e) Wu, Y. P.; Zhang, B. T. Guo, L.-H. *Anal. Chem.* **2013**, *85*, 6908−6914.

(5) Liu, S. L.; Li, C.; Cheng, J.; Zhou, Y. X. *Anal. Chem.* **2006**, *78*, 4722–4726.

(6) (a) Lamansky, S.; Djurovich, P.; Murphy, D.; Abdel-Razzag, F.; Lee, H. E.; Adachi, C.; Burrows, P. E.; Forrest, S. R.; Thompson, M. E. *J. Am. Chem. Soc.* **2001**, *123*, 4304−4312. (b) You, Y. M.; Park, S. Y. *J. Am. Chem. Soc.* **2005**, 127, 12438−12439. (c) Yang, C.-H.; Cheng, Y. M.; Chi, Y.; Hsu, C. J.; Fang, F.-C.; Wong, K.-T.; Chou, P.-T.; C.-H. Chang, C.-H. Tsai, M.-H.; Wu, C.-C. *Angew. Chem. Int. Ed.* **2007**, *46*, 2418–2421.

(7) (a) Kim, J. I.; Shin, I.-S.; Kim, H.; Lee, J.-K.; *J. Am. Chem. Soc.* **2005**, *127*, 1614−1615. (b) Li, C. H.; Lin, J.; Guo, Y. S.; Zhang, S. S. *Chem. Commun.* **2011**, 47, 4442–4444. (c) Li, M.-J.; Jiao, P. C.; Lin, M.; He, W. W.; Chen, G.-N.; Chen, X. *Analyst* **2011**, *136*, 205−210.

(8) (a) Borisov, S. M.; Klimant, I. *Anal. Chem.* **2007**, *79*, 7501–7509. (b) Liu, J. L.; Liu, Y.; Liu, Q.; Li, C. Y.; Sun, L. N.; Li, F. Y. *J. Am. Chem. Soc.* **2011**, 133, 15276–15279. (c) Ma, D.-L.; Wong, W.-L.; Chung, W.-H.; Chan, F.-Y.; So, P.-K.; Lai, T.-S.; Zhou, Z.-Y.; Leung, Y.-C.; Wong, K.-Y. *Angew. Chem. Int. Ed.* **2008**, *47*, 3735–3739.

(9) Goff, A. L.; Cosnier, S. *J. Mater. Chem.* **2011**, *21*, 3910–3915.

(10) (a) Metcalfea, C.; Thomas, J. A. *Chem. Soc. Rev.* **2003**, *32*, 215–224. (b) Erkkila, K. E.; Odom, D. T.; Barton, J. K. *Chem. Rev.* **1999**, *99*, 2777–2795. (c) Lo, K. K.-W.; Chung, C.-K.; Zhu, N. Y. *Chem. Eur. J.* **2006**, *12*, 1500–1512. (d) Liu, H.-K.; Sadler, P. J. *Accounts Chem. Res.* **2011**, *44*, 349–359.

(11) Dong, T.-Y.; HWang, M.-Y.; Hsu, T.-L.; Schei, C.-C.; Yeh, S.-K. *Inorg. Chem.* **1990**, *29*, 80–85.

(12) (a) Greguric, A.; Greguric, I. D.; Hambley, T. W.; Aldrich-Wright, J. R.; Collins, J. G. *Dalton Trans.* **2002**, 849–855. (b) Yamada, M.; Tanaka, Y.; Yoshimoto, Y.; Kuroda, S.; Shimao, *I. Bull. Chem. Soc. Jpn.* **1992**, *65*, 1006–1011.

(13) Nonoyama, M. *Bull. Chem. Soc. Jpn.* **1974**, *47*, 767–769.

(14) Grabar, K. C.; Smith, P. C.; Musick, M. D.; Davis, J. A. D.; Walter, G.; Jackson, M. A.; Guthrie, A. P.; Natan, M. J. *J. Am. Chem. Soc.* **1996**, *118*, 1148–1153.

(15) (a) Sprouse, S.; King, K. A.; Spellane, P. J.; Watts, R. J. *J. Am. Chem. Soc.* **1984**, *106*, 6647–6653. (b) Pavlik, J. W.; Connors, R. E.; Burns, D. S.; Kurzweil, E. M. *J. Am. Chem. Soc.* **1993**, *115*, 7645–7652. (c) Colombo, M. G.; Brunold, T. C.; Riedener, T.; Gudel, H. U. *Inorg. Chem.* **1994**, *33*, 545–550. (d) Tamayo, A. B.; Alleyne, B. D.; Djurovich, P. I.; Lamansky, S.; Tsyba, I.; Ho, N. N.; Bau, R.; Thompson, M. E. *J. Am. Chem. Soc.* **2003**, *125*, 7377–7387. (e) Waern, J. B.; Desmarets, C.; Chamoreau, L.-M.; Amouri, H.; Barbieri, A.; Sabatini, C.; Ventura, B.; Barigelletti F. *Inorg. Chem.* **2008**, *47*, 3340−3348.

(16) Robinson, M. R.; O'Regan, M. B.; Bazan, G. C. *Chem. Commun.* **2000**, 1645–1646.

(17) (a) Lo, K. K.-W.; Lee, P.-K.; Lau, J. S.-Y. *Organometallics* **2008**, *27*, 2998–3006. (b) Lo, K. K.-W.; Chung, C.-K.; Lee, T. K.-M.; Lui, L.-H.; Tsang, K. H.-K.; Zhu, N. *Inorg. Chem.* **2003**, *42*, 6886–6897. (c) Lo, K. K.-W.; Lau, J. S.-Y. *Inorg. Chem.* **2007**, *46*, 700–709. (d) Lo, K. K.-W.; Zhang, K. Y.; Chung, C.-K.; Kwok, K. Y. *Chem. Eur. J.* **2007**, *13*, 7110–7130. (e) Avilov, I.; Minoofar, P.; Cornil, J.; De Cola, L. *J. Am. Chem. Soc.* **2007**, *129*, 8247–8258.

(18) (a) Vaes, A.; Van der Auweraer, M.; Bosmans, P.; De Schryver, F. C. *J. Phys. Chem. B* **1998**, *102*, 5451–5459. (b) Wu, D.-G.; Huang, C.-H.; Gan, L.-B.; Zheng, J.; Huang, Y.-Y.; Zhang, W. *Langmuir* **1999**, *15*, 7276–7281.

(19) (a) Jiang, K.; Xie H.; Zhan, W. *Langmuir* **2009**, *25*, 11129–11136. (b) Ju, C.-C.; Zhang, A.-G.; Sun, H.-L.; Wang, K.-Z. Organometallics 2011, 30, 712–716.

(20) Meng, T.-T.; Zheng, Z.-B.; Wang, K.-Z. *Langmuir* **2013**, *29*, 14314−14320.

(21) (a) Bard, A. J.; Faulker, L. R. *Elctrochemical Methods Fundamentals and Applications; Wiley: New York,* **1980**. (b) Yuan, Y.-J.; Yu, Z.-T.; Gao, H.-L.; Zou Z.-G.; Zheng, C.; Huang W. *Chem. Eur. J.* **2013**, *19*, 6340– 6349.

(22) (a) Cai, J.-G.; Yu, Z.-T.; Yuan, Y.-J.; Li, F.; Zou Z.-G. *ACS Catal.* **2014**, *4*, 1953−1963. (b) Yuan, Y. J.; Yu, Z. T.; Chen, X. Y.; Zhang, J. Y.; Zou, Z. G. *Chem. Eur. J.* **2011**, *17*, 12891−12895. (c) Yuan, Y. J.; Zhang, J. Y.; Yu, Z. T.; Feng, J. Y.; Luo, W. J.; Ye, J. H.; Zou, Z. G. *Inorg. Chem.* **2012**, *51*, 4123−4133.

(23) (a) Palmer, J. H.; Day, M. W.; Wilson, A. D.; Henling, L. M.; Gross, Z.; Gray, H. B. *J. Am. Chem. Soc.* **2008**, *130*, 7786–7787. (b) Neubauer, A.; Grell, G.; Friedrich, A.; Bokarev, S. I.; Schwarzbach, P.; Gärtner, F.; Surkus, A.-E.; Junge, H.; Beller, M.; Kühn, O.; Lochbrunner, S. *J. Phys. Chem. Lett.* **2014**, *5*, 1355−1360.

(24) (a) Kim, Y. S.; Liang, K.; Law, K. Y.; Whitten, D. G. *J. Phys. Chem.* **1994**, *98*, 984–988. (b) Fushimi, T.; Oda, A.; Ohkita, H.; Ito, S. *Langmuir* **2005**, *21*, 1584–1589.

(25) (a) Dirks, R. M.; Pierce, N. A. *Proc. Natl. Acad. Sci. U.S.A.* **2004**, *101*, 15275−15278. (b) Chen, Y.; Xu, J.; Su, J.; Xiang, Y.; Yuan, R.; Chai, Y. Q. *Anal. Chem.* **2012**, *84*, 7750−7755. (c) Huang, J.; Wu, Y. R.; Chen, Y.; Zhu, Z.; Yang, X. H.; Yang, C. J.; Wang, K. M.; Tan, W. H. *Angew. Chem. Int. Ed.* **2011**, *50*, 401−404. (d) Wang, F. A.; Elbaz, J.; Orbach, R.; Magen, N.; Willner, I. *J. Am. Chem. Soc.* **2011**, *133*, 17149−17151.

(26) Zang, Y.; Lei, J. P.; Zhang, L.; Ju, H. X. *Anal. Chem.* **2014**, *86*, 12362–12368.

For TOC only

Cyclometalated Iridium Complex-Based Label-Free Photoelectrochemical Biosensor for DNA Detection by Hybridization Chain Reaction Amplification

Chunxiang Li, Hongyang Wang, Jing Shen, Bo Tang*